Front. Earth Sci. 2022, 16(1): 121–131
https://doi.org/10.1007/s11707-020-0865-6

RESEARCH ARTICLE

Drastic change in dynamics as Typhoon Lekima experiences an eyewall replacement cycle

Fen XU[1], X. San LIANG (✉)[1,2]

1 School of Atmospheric Sciences, Nanjing University of Information Science and Technology, Nanjing 210044, China.
2 School of Marine Sciences, Nanjing University of Information Science and Technology, Nanjing 210044, China

Abstract Why does the 1909 typhoon, Lekima, become so destructive after making landfall in China? Using a newly developed mathematical apparatus, the multiscale window transform (MWT), and the MWT-based localized mutliscale energetics analysis and theory of canonical transfer, this study is intended to give a partial answer from a dynamical point of view. The ECMWF reanalysis fields are first reconstructed onto the background window, the TC-scale window, and the convection-scale window. A localized energetics analysis is then performed, which reveals to us distinctly different scenarios before and after August 8–9, 2019, when an eyewall replacement cycle takes place. Before that, the energy supply in the upper layer is mainly via a strong upper layer-limited baroclinic instability; the available potential energy thus-gained is then converted into the TC-scale kinetic energy, with a portion to fuel Lekima's upper part, another portion carried downward via pressure work flux to maintain the cyclone's lower part. After the eyewall replacement cycle, a drastic change in dynamics occurs. First, the pressure work is greatly increased in magnitude. A positive baroclinic transfer almost spreads throughout the troposphere, and so does barotropic transfer; in other words, the whole air column is now both barotropically and baroclinically unstable. These newly occurred instabilities help compensate the increasing consumption of the TC-scale kinetic energy, and hence help counteract the dissipation of Lekima after making landfalls.

Keywords Typhoon Lekima, multiscale window transform, canonical transfer, multiscale energetics, barotropic/baroclinic instability

Received May 20, 2020; accepted December 23, 2020

E-mail: sanliang@courant.nyu.edu

1 Introduction

The 1909 typhoon, Lekima, as the strongest landfall typhoon in China in 2019, enters the history on August 4, 2019 9:00 am UTC. It forms over the North-western Pacific Ocean and then rapidly intensifies as it moves north-westward. On August 7, it attains the intensity of super strong typhoon, and makes landfall on August 9, in Wenling, Zhejiang, China, with a maximum wind speed of 52 m/s. After staying in Zhejiang for 20 h, this devastating typhoon gradually weakens, moving northward through Jiangsu and the Yellow Sea. Lekima makes a second landfall in Qingdao, Shandong, China, on August 11th, 2019, with a maximum wind of 23 m/s. It gradually weakens thenafter, and finally decays over the Bohai Sea (Fig. 1). Lekima is special in that it has a relatively long lifecycle (9 days) and has stayed for 44 h over Chinese mainland. The long duration on land has dragged the most developed provinces along the eastern coast of China such as Zhejiang, Jiangsu, Shandong, etc., into the midst of a catastrophic disaster, leading to 56 people dead and 14 others missing, and an economic loss of at least 53.72 billion yuan.

Much effort has been invested in understanding the dynamics underlying tropical cyclones. They have been particularly studied within the frameworks of conditional instability of second kind (CISK) (Charney and Eliassen, 1964), wind-induced surface heat exchange (WISHE) (Emanuel, 1986, 1989), vortical hot tower route to tropical cyclogenesis (VHT) (Hendricks et al., 2004; Montgomery et al., 2006, 2009), and the top-down (Bister and Emanuel, 1997) and bottom-up (Zhang and Bao, 1996) genesis. Luo (2005) pointed out that multi-scaleness and nonlinearity are the most essential controlling factors in typhoon dynamics. He hence has done much work in this regards in the fields of, say, self-organization, fractals, to name a few (Luo, 2005; Luo et al., 2014). Nonetheless, many issues are yet to be resolved. For example, how the local system is

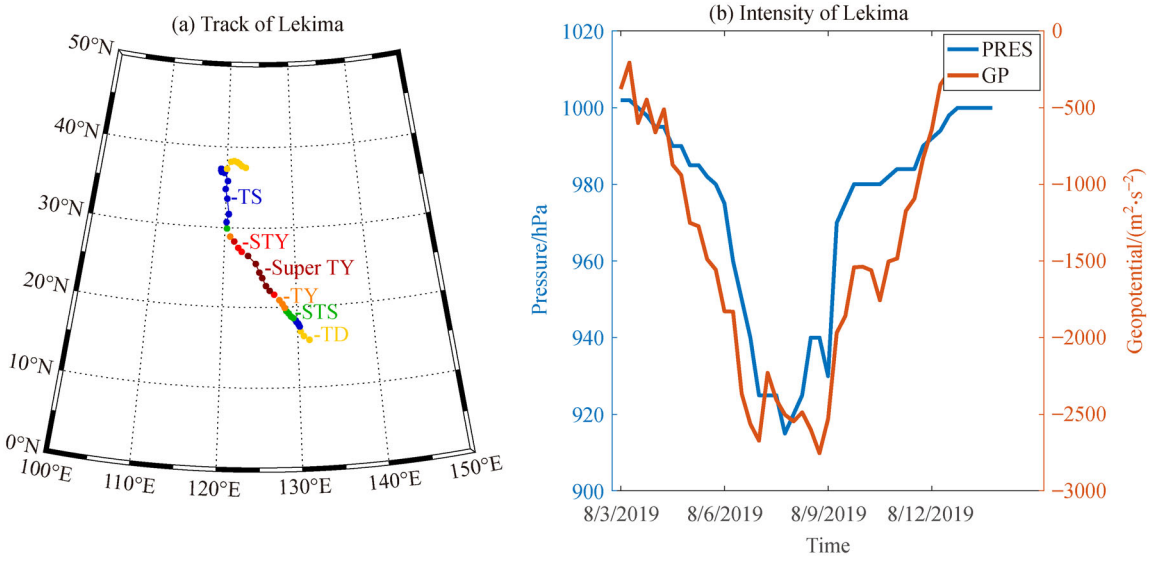

Fig. 1 (a) The track of Typhoon Lekima. Data source: China Meteorological Administration (CMA) Tropical Cyclone Data Center (CMA Tropical Cyclone Data Center website). (b) The minimum pressure near the typhoon center (blue line) and the minimum geopotential at 1000-hPa near the typhoon center.

dynamically maintained as it runs through a variable ambient environment is still a mystery. An outstanding question is: TCs usually involve eye wall replacement cycles, which may exert very important impact on the intensity and path of them; how does a mobile cyclone respond to this replacement, then? The complexity of the processes lies in that the cyclone is not alone in the atmospheric system; it interacts upward in the spectrum with a favorable large-scale environment, and downward with cumulus convections. Historically, Gray (1968) first observed that the generation of tropical cyclones relies on a suitable ambient environment, including "sufficiently warm sea surface temperature, atmospheric instability, high humidity in the lower to middle levels of the troposphere, enough Coriolis force to develop a low pressure center, a pre-existing low level focus or disturbance, and low vertical wind shear." On the other hand, it has been reported that tropical cyclogenesis may be triggered by meso-scale processes such as mesoscale convection systems or mesoscale eddies (Riehl, 1954; Simpson et al., 1997; Cheung, 2004; Ma and Tan, 2009; Fei et al., 2011). Besides, boundary layer (Zhang et al. 2008 and 2017), air-sea interaction (Ma et al., 2013; Liu et al., 2011), monsoon troughs (Zong and Wu, 2015; Wu and Duan, 2015), tropical upper tropospheric troughs (Montgomery and Farrell, 1993; Mcbride and Keenan, 1982), easterly waves (Molinari et al., 2010), Madden-Julian oscillation (MJO) (Maloney and Hartmann, 2001), etc., may also play important roles, and may be regarded as external disturbance sources. In short, interactions with the ambient through multiscale processes hence form the key to the problem.

To investigate the multiscale interactions underlying meteorological phenomena, dynamical diagnostics make an important methodology. Particularly, the Lorenz energy cycle diagnostics prove to be a powerful approach. However, tropical cyclogenesis has been rarely studied this way (Ooyama, 1982; Yu, 1999; Yu and Wu, 2001; Papin, 2011; Duan et al., 2016;), making it difficult to explore those dynamical processes such as barotropic and baroclinic instabilities, a concept established within the framework of multiscale energetics. This is perhaps due to the processes highly localized in space (spatially limited and mobile) and nonstationary in time (energy burst), which pose great challenges to the classical multiscale energetics analysis. During the past decade these problems have been systematically addressed, with a new functional analysis machinery, namely, multiscale window transform (MWT), constructed, and a MWT-based diagnostic methodology developed. In this study, we present an application of this methodology, in the hope of enriching our understanding of tropical cyclones through investigating the variation of the dynamics underlying Lekima, the super strong typhoon which has incurred a huge damage to China, as it moves. In the following we first briefly introduce the methodology, then the data set. After that are the results. Section 7 summarizes the study.

2 Methods

2.1 Multiscale window transform

The research methodology for this study is the multiscale window transform (MWT) by Liang and Anderson (2007), and the MWT-based theory of canonical transfer (Liang

2016) and localized multiscale energy and vorticity analysis (MS-EVA) by Liang and Robinson (2005). This section is just a very brief introduction of the concepts; more details are referred to Liang and Anderson (2007) and Liang (2016).

MWT is a tool decomposes a function space into a direct sum of orthogonal subspaces, each with an exclusive range of scales, while retaining the locality of the resulting multiscale energies. Such a subspace is called a scale window, or simply a window. Given a scale window ϖ, for a time series $T(t)$, it can be reconstructed onto the window, written $T^{\sim\varpi}(t)$ (this is just like a filtered series). In the mean time, we have a transform coefficient, written $\hat{T}_n^{\sim\varpi}$ ($(\hat{\cdot})_n^{\sim\varpi}$ denotes MWT on window ϖ at time step n). The multiscale energy on window ϖ is then $\left[\hat{T}_n^{\sim\varpi}\right]^2$ (up to some multiplier). Note: it is by no means the square of the filtered field $\left[\hat{T}^{\sim\varpi}(t)\right]^2$, a common mistake in the filter-based multiscale energetics studies! This is where MWT is completely different from the traditional filters.

In MWT, a scale window is demarcated by two scale levels, or window bounds, in the wavelet spectrum. Given a series $T\{(t)\}$ with a duration τ, a scale level j corresponds to a period $2^{-j}\tau$. In this study we need three scale windows, which are bounded above by three scale levels: j_0, j_1 and j_2, or by three time scale bounds $2^{-j_0}\tau$, $2^{-j_1}\tau$ and $2^{-j_2}\tau$. For easy reference, they will be referred to as large-scale window, tropical cyclone-scale window (or simply cyclone window, TC window), and cumulus convection-scale window (or convection window). In the following, they may also be denoted by $\varpi = 0,1,2$ respectively.

2.2 Canonical transfer and multiscale energetics analysis

We are now following Liang (2016) to apply MWT to the equations that govern the atmospheric motions. Consider the primitive equations in an isobaric coordinate frame:

$$\frac{\partial v_h}{\partial t} + v_h\cdot\nabla_h v_h + \omega\frac{\partial v_h}{\partial p} + fk\times v_h = -\nabla_h\Phi + F_{m,p} + F_{m,h}, \tag{1}$$

$$\frac{\partial\Phi}{\partial p} = -\alpha, \tag{2}$$

$$\nabla_h\cdot v_h + \frac{\partial\omega}{\partial p} = 0, \tag{3}$$

$$\frac{\partial T}{\partial t} + v_h\cdot\nabla_h T + \omega\frac{\partial T}{\partial p} + \omega\overline{\alpha}\frac{L-L_\mathrm{d}}{g} + \omega\alpha\frac{L-L_\mathrm{d}}{g} = \frac{\dot{q}_\mathrm{net}}{c_p}, \tag{4}$$

$$\alpha = \frac{R}{p}T, \tag{5}$$

where L is the lapse rate and L_d the lapse rate for dry air, and the overbar stands for mean over time (from 23 January 2019, 16:00UTC to 31 December 2019, 23:00 UTC) and over the horizontal isobaric plane (0–50°N, 105°E–150°E). The other notations are conventional. Note here Φ and α are anomalies; their time averages have been removed a priori. The kinetic energy (KE) and available potential energy (APE) on scale windows $\varpi = 0, 1, 2$ are

$$K^\varpi = \frac{1}{2}\hat{v}_h^{\sim\varpi}\cdot\hat{v}_h^{\sim\varpi},$$

$$A^\varpi = \frac{1}{2}c\left(\hat{T}^{\sim\varpi}\right)^2,$$

where $c = \dfrac{g}{\overline{T}(g/c_p - L)}$. Liang (2016) showed that, in a symbolic way,

$$\frac{\partial K^\varpi}{\partial t} + \nabla\cdot Q_K^\varpi = \Gamma_K^\varpi - \nabla\cdot Q_P^\varpi - b^\varpi + F_K^\varpi, \tag{6}$$

$$\frac{\partial A^\varpi}{\partial t} + \nabla\cdot Q_A^\varpi = \Gamma_A^\varpi + b^\varpi + \mathrm{S}_A^\varpi + F_A^\varpi, \tag{7}$$

where F_K^ϖ and F_A^ϖ are works done through eddy dissipation and diffusion, respectively (external forcings are also embedded). They are usually represented through parameterization and hence do not have explicit expressions. The expressions and physical meanings of other terms are summarized in Table 1 (the time step n is suppressed for notational simplicity). Schematized in Fig. 2 is the relationship between them that forms a flow path. Here the most important ones are the Γ terms, which signify the energy transfers between different scale windows, hence the internal processes that lead to the formation and decay of the tropical cyclones. It should be noted that they are very different from those in classical formalisms. Particularly, there exists for them a very important property; that is

$$\sum\nolimits_\varpi\left(\sum\nolimits_n\Gamma_n^\varpi\right) = 0, \tag{8}$$

(now n is supplied) (Liang, 2016). That is to say, energy transfer process is a mere redistribution of energy among the scale windows, without generating or destroying energy as a whole. This property, though simply stated, does not hold in previous time decomposition-based or Lorenz-type energetics formalisms (see below). To distinguish, such as transfer is termed "canonical transfer". A canonical transfer has a Lie bracket form that satisfies the Jacobian identity, reminiscent of the Poisson bracket in Hamiltonian mechanics; see Liang (2016) for details.

MWT and the MWT-based theory of canonical transfer have been well applied in many fields in meteorology and

Table 1 Expressions and physical meanings of the energetic terms in Eqs. (6)–(7). If total energetics (in W) are to be computed, the resulting integrals with respect to (*x, y, p*) should be divided by *g*. Besides, all terms are to be multiplied by 2^{j_2}, which is omitted for notational simplicity. The colon operator is defined, for vectors *A, B, C, D*, such that $AB : CD = (A \cdot B)(C \cdot D)$.

Symbol	Expression	Physical meaning
K^{ϖ}	$\frac{1}{2}\hat{\boldsymbol{v}}_h^{\sim\varpi} \cdot \hat{\boldsymbol{v}}_h^{\sim\varpi}$	KE on scale window ϖ
Q_K^{ϖ}	$\frac{1}{2}\widehat{(\boldsymbol{v}\boldsymbol{v}_h)}^{\sim\varpi} \cdot \hat{\boldsymbol{v}}_h^{\sim\varpi}$	Flux of KE on window ϖ
Γ_K^{ϖ}	$\frac{1}{2}[\widehat{(\boldsymbol{v}\boldsymbol{v}_h)}^{\sim\varpi} : \nabla\hat{\boldsymbol{v}}_h^{\sim\varpi} - \nabla\widehat{(\boldsymbol{v}\boldsymbol{v}_h)}^{\sim\varpi} \cdot \hat{\boldsymbol{v}}_h^{\sim\varpi}]$	Canonical transfer of KE to window ϖ
Q_P^{ϖ}	$\hat{\boldsymbol{v}}^{\sim\varpi}\hat{\Phi}^{\sim\varpi}$	Pressure flux
b^{ϖ}	$\hat{\omega}^{\sim\varpi}\hat{\alpha}^{\sim\varpi}$	Buoyancy conversion
A^{ϖ}	$\frac{1}{2}c(\hat{T}^{\sim\varpi})^2, c = \frac{g}{\overline{T}(g/C_p - L)}$	APE on scale window ϖ
Q_A^{ϖ}	$\frac{1}{2}c\hat{T}^{\sim\varpi} \cdot \widehat{(\boldsymbol{v}T)}^{\sim\varpi}$	Flux of APE on window ϖ
Γ_K^{ϖ}	$\frac{c}{2}[\widehat{(\boldsymbol{v}T)}^{\sim\varpi} \cdot \nabla\hat{T}^{\sim\varpi} - \hat{T}^{\sim\varpi}\nabla \cdot \widehat{(\boldsymbol{v}T)}^{\sim\varpi}]$	Canonical transfer of APE to window ϖ
S_A^{ϖ}	$\frac{1}{2}\hat{T}^{\sim\varpi}\widehat{(\omega T)}^{\sim\varpi}\frac{\partial c}{\partial p} + \frac{1}{\overline{T}}\widehat{\omega\alpha}^{\sim\varpi}$	Apparent source/sink (usually negligible)

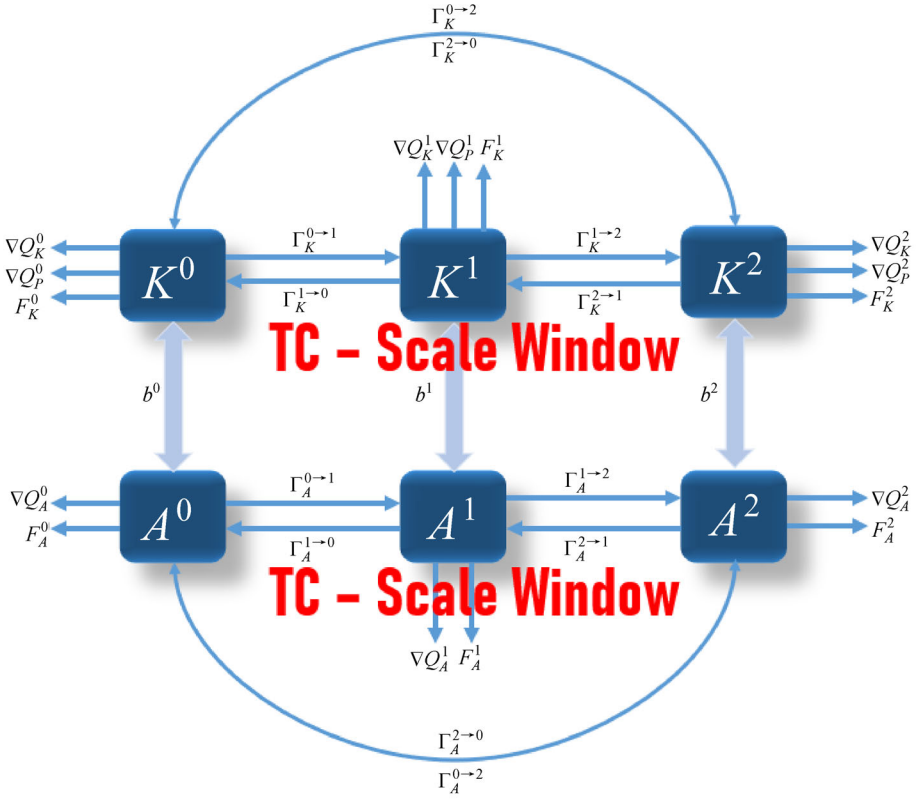

Fig. 2 A schematic of the multiscale energy pathway for a three-window decomposition (the scale windows are denoted in the superscripts as 0, 1, and 2, respectively).

Notes: a canonical transfer to a window ϖ may involve contributions from different windows; we need to differentiate them to trace the dynamical source. Details are referred to Liang and Robinson (2005). Here we just use the superscript notation $\varpi_1 \to \varpi_2$ to signify the transfer from window ϖ_1 to ϖ_2. It has been rigorously proved by Liang and Robinson (2007) that $\Gamma_A^{0\to1}$ provides a quantitative measure of the baroclinic instability of the mean flow, while $\Gamma_K^{0\to1}$ provides a barotropic instability measure. For convenience, in the following we will write them as BC and BT, and may refer to them baroclinic transfer and barotropic transfer, respectively.

oceanography. Examples include storm track dynamics (Zhao and Liang, 2018, 2019; Zhao et al., 2018), atmospheric blocking (Ma and Liang, 2017; Li et al., 2020), sudden stratospheric warming (Xu and Liang, 2017), Kuroshio Extension (Yang and Liang, 2016), Gulf of Mexico eddy shedding (Yang et al., 2020), to name a few.

3 Data

The European Centre for Medium-Range Weather Forecasts (ECMWF) reanalysis data ERA5, including temperature, geopotential, and wind (u, v, ω), are used for the diagnostics in this study. The reanalysis fields have a resolution of 0.25°×0.25° in horizontal and a resolution of 1 h in time. We choose a domain covering 0°–50°N, 105°E–150°E, with 28 levels in the vertical (1000 hPa–70 hPa), and a period from 16:00 on January 23, 2019 to 23:00 at December 31, 2019, which totals 2^{13} = 8192 h (a power of 2 is needed for the analysis; see Section 2.1). Due to the limited resolution, the ERA5 data do not resolve well the structure of the eyewall, but the intensity and circulation of Lekima are very well represented. We have compared the track and intensity derived from the ERA5 data to the best track data from the China Meteorological Administration (CMA) Tropical Cyclone Data Center (Ying et al. 2014). Note that the ERA5 data are in isobaric coordinates and we have to choose the 1000-hPa geopotential as a substitute for pressure in the comparison; that is to say we choose the value of the 1000-hPa minimum geopotential near the typhoon center to represent the intensity of the typhoon, and its location as the track. The results show that the two tracks are almost the same (not shown). We have also compared its intensity, and the results are shown in Fig. 1(b). Obviously their evolutionary trends are the same, although the two lines (Fig. 1(b)) do not completely overlap. For all that account, this data set serves our purpose very well. Particularly, the resolution is enough, considering that our focus is not on the eyewall structure itself.

4 MWT setup

First we need to determine the scale window bounds (scale level) j_0, j_1, and j_2 for the multiscale energetics analysis, The time span for this study is from 16:00 on January 24 to 23:00 on December 31, 2019, which totals 2^{13} steps with a stepsize of 1 h (recall that the number of time steps is required to be a power of 2). This way Lekima is made to lie in the middle of the series to avoid any possible boundary effect from the transform. In this study, the original fields are reconstructed with MWT onto three scale windows, namely, the background window, tropical cyclone-scale window (cyclone window or TC window), and convection scale window. After many trials, the following parameters are set: $j_0 = 4$, $j_1 = 9$, $j_2 = 13$. That gives a TC window for Lekima in time domain as 16–512 h (i.e., 0.67–21.3 days). The criterion here is whether the tropical cyclone can be clearly separated from the background and the convections. We have also tried many other parameters but this combination produces the best result.

5 Lekima reconstructed with the multiscale window transform

The multiscale reconstructed geopotential fields $\Phi^{\sim\varpi}$ (ϖ = 0, 1, 2) at 850hPa are shown in Fig. 3. On the background window (the upper row, Figs. 3(a)–3(e)), $\Phi^{\sim 0}$ evolve rather slowly, with a low over the land, two lows over the ocean, and the subtropical high to the east. On the TC-scale window, the tropical cyclone signal is very clear (middle row, Figs. 3(f)–3(j)). It should be mentioned here that the 1910 TC, namely, Krosa, has formed by August 6 to the east of Lekima, so we actually see two cyclones evolving in tandem with each other. The geopotential height $\Phi^{\sim 2}$ on the convection window (bottom row, Figs. 3(k)–3(o)) looks rather chaotic, without significantly clear structure.

The evolution of the TC-scale geopotential $\Phi^{\sim 1}$ at 300 hPa, 500h Pa and 850 hPa from August 4–12, 2019, presents more information (not shown). On August 4 at 9:00, there appears near (17°N, 130.4°E) a low pressure center (tropical cyclone) on the 850-hPa. This is Lekima, which then develops rapidly. On August 7, it attains over Ryukyu Archipelago the intensity of super strong typhoon. It keeps moving north-westward to the mainland of China, making landfall on August 9 in Wenling, Zhejiang. After that, it moves northward along the eastern coast of China, crossing the Yellow Sea and makes another landfall in Qingdao, Shandong, China, at 12:00 on August 11. Since then, it gradually weakens, as can be seen on the map on August 12. Note another TC called Krosa has been staying throughout to the east in the west Pacific. In this study we focus on Lekima only.

Compared to 850 hPa, the evolution of "Lekima" at 300 hPa and 500 hPa seems to lag behind. On August 4, the tropical cyclone signal at 300 hPa and 500 hPa is almost indiscernible, while it has been clear at 850-hPa. On August 10, it is merged into a low pressure system in the Huang-Huai area of China at 20 o'clock, and becomes an extratropical cyclone. At the time when it begins to weaken at 300 hPa, it is still robust at 850 hPa. From these observations, Lekima seems to form from bottom, and decay from top. If we look into the details of the convection-scale geopotential height, indeed a low pressure center emerges on August 4 at 3 am, and begins to develop ever since (not shown). From 4 am to 9 am on the same day the center can be clearly seen on the map.

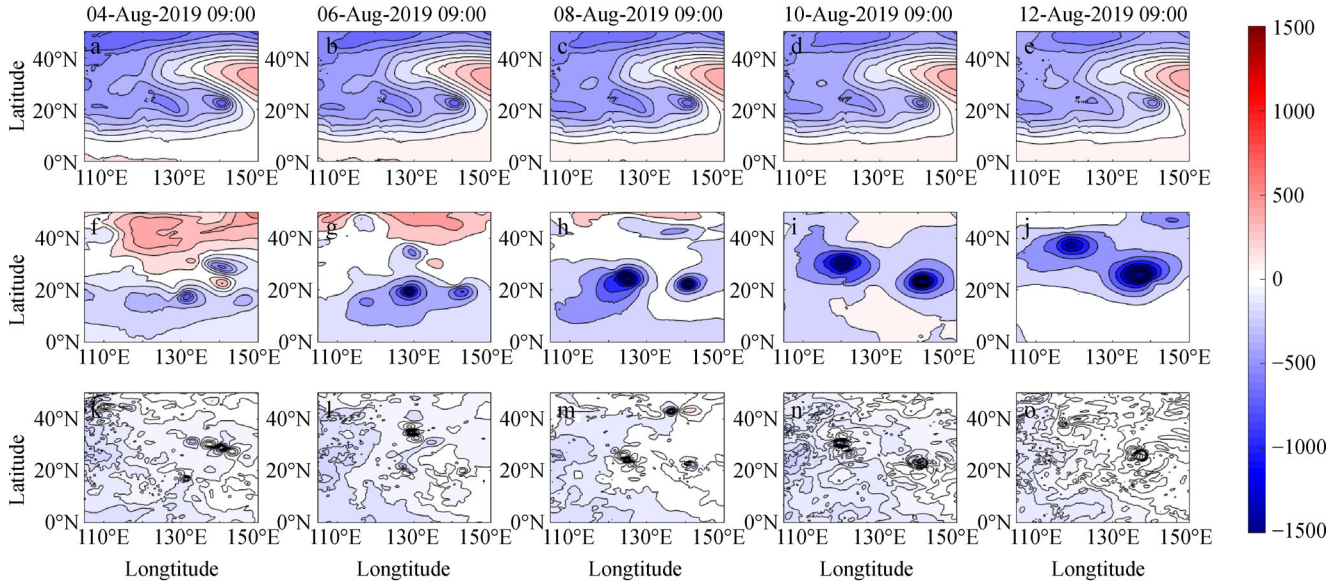

Fig. 3 The multiscale reconstructed geopotential fields (unit: $m^2 \cdot s^{-2}$) form August 4 to August 12, 2019 at 850 hPa. The plots from upper to bottom are for the background window, TC window, and convection window, respectively.

6 Multiscale energy cycles

6.1 Horizontal distribution of the canonical transfer and buoyancy conversion

In Section 2 we remarked that two fundamental and challenging issues in multiscale analysis are, 1) the representation of energy on scale windows; 2) the derivation of energy transfer across the scale windows. For the former, it is actually a difficult problem in functional analysis which, unfortunately, has been totally overlooked (and treated as trivial) in the atmosphere-ocean science during the past 20–30 years. It has been shown that the traditional filtering-based formalisms are inappropriate in that squaring a filtered variable does not result in a physically meaningful notion of energy at all. For 2), a theory of canonical transfer has been established to allow us to gain insight into how energy redistributes to generate new patterns. An appealing property, among others, is that it automatically guarantees energy conservation in the course of multiscale interaction, in contrast to the classical formalisms used thus far; other properties include a Lie bracket form for the formula, which is reminiscent of the Poisson bracket in theoretical physics (Liang, 2016). In short, this is the first rigorous formalism that allows us to probe, in a faithful way, into the internal nonlinear dynamical processes which would otherwise impossible to investigate. Indeed, since its advent, the MWT-based multiscale energetics analysis and the theory of canonical transfer have been successfully applied to the studies of a large variety of atmospheric, oceanic and engineering flow problems; some most recent ones include Ma and Liang (2017), Zhao et al. (2019), Yang et al. (2020), to name a few.

As already established in a series of theoretical and application papers ever since 2002, canonical transfer is of central importance in geophysical fluid dynamics in that it regulates the internal processes of atmospheric motions on one scale that lead to the formation of meteorological patterns on another (e.g., Liang and Robinson, 2007; Liang, 2016). In the context of this study, let us look at the transfers between the background window and TC window. The canonical transfer of APE, $\Gamma_A^{0\to1}$, and that of KE, $\Gamma_K^{0\to1}$, are respectively related to the two fundamental notions, namely, baroclinic instability and barotropic instability. A positive sign indicates that the system is locally unstable, and, moreover, the magnitude gives the desired growth rate (Liang and Robinson, 2007). For convenience we will henceforth call them baroclinic transfer and barotropic transfer, or BC and BT for short. Here a positive BC/BT means that the TC-scale window gains APE/KE from the background.

In this study, the computational results show that along the track there always exists a positive center of BC, which does not disappear until the typhoon disappears. This positive center indicates that a baroclinic instability is occurring there, i.e., that the TC-scale APE is mainly from the background window. In other words, Lekima builds up its thermal structure via a baroclinic instability, which, through buoyancy conversion, also influence its dynamical processes. This instability is particularly clear at upper levels, leading to the formation of the warm core there. Moreover, this canonical transfer becomes strengthened after Lekima makes landfall, making it a very devastating

TC ever landed in China. We will discuss this more in detail later. Compared to BC, BT is much weaker (not shown). Its signal, however, becomes more pronounced after Lekima makes landfall. Whether in the lower or upper layers, along the track of Lekima we can see a positive center, which means that KE is transferred from the background window to the TC window. That is to say, the TC is refueled after making landfall via a barotropic instability. That is another reason why Lekima becomes so devastating.

It is also noticeable that, through the whole air column, there is a mixed instability after the landfall. That is to say, the whole air column is now both barotropically and baroclinically unstable. This is in contrast to that prior to the landfall, when only baroclinic instability is observed in the upper layer. Based on these observations, it is clear that baroclinic instability makes a mechanism for Lekima's development, whearas a mixed instability supplies the energy for Lekima to maintain.

As those between the background and TC scale windows, the canonical transfers between the TC window and the convection window are of equal importance. The instabilities for the local system, i.e., the TC, are essentially related to the canonical transfers $\Gamma_K^{2\to1}$ and $\Gamma_A^{2\to1}$, and will be referred to secondary instabilities. Though $\Gamma_A^{0\to1}$ is smaller than $\Gamma_K^{2\to1}$ (not shown), during the life cycle of Lekima it is significant along the path, and has a clear localized structure. This structure is more pronounced in lower layers. So the dynamically Lekima also gains kinetic energy from the convective window; that the role of the cumulus convective processes cannot be neglected. Another canonical transfer, $\Gamma_A^{2\to1}$ (not shown), is by comparison insignificant. It only shows a weak signal in the upper layer.

As can be transferred between different scale windows, energy can also be converted from one type to another within the same scale window. In geophysical fluid dynamics, this is the buoyancy conversion process between KE and APE (the expression is shown in Table 1). The buoyancy conversion on the TC-scale window, b^1, with a negative value signifying from a conversion from the TC-scale APE to the TC-scale KE. From it we can see a conspicuous negative center in accordance with the cyclone (not shown). Its strength is much larger in upper layers (cf. Fig. 5(e)), indicating the vertical asymmetry as shown before in the BC distribution. Recalling the BC evolution mentioned above, the TC-scale APE converted to the TC-scale KE comes from the background window through baroclinic instability, and this is particularly the case in the upper layer. This part of the TC-scale APE that is converted is used to fuel the motion, while the retained part maintains the warm-core of the cyclone.

6.2 Vertical structures of the energetics

To have a clear view of the evolutionary vertical structure of the typhoon, we integrate the TC-scale energetics at each level over the cyclonic area. As the cyclone is on the move, so is the integration domain. Here the integrations have taken into account the weights with latitudes. We choose 09:00 as the instance to represent each day. Displayed in Fig. 4 are the resulting TC-scale APE and KE.

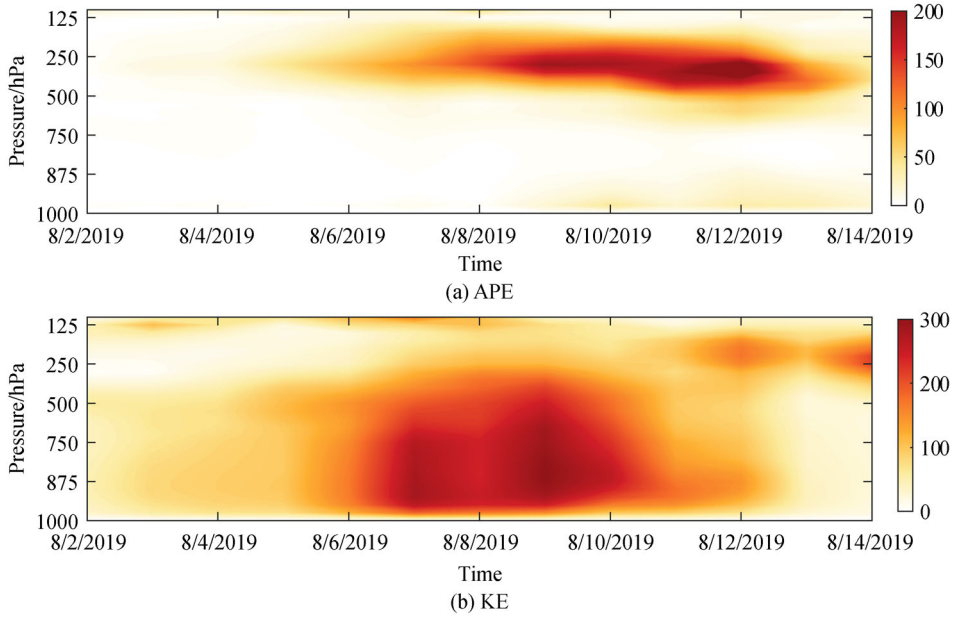

Fig. 4 Time-pressure distributions of the horizontally integrated (a) TC window APE and (b) TC window KE. We choose 09:00 UTC as the instance to represent each day. The space window is a square centered at the TC center, with a side length of 6° (latitude and longitude); same below.

As we can see, the TC-scale APE is mainly concentrated in the upper layers, i.e., the warm core is stronger in the upper layers, while the TC-scale KE is distributed throughout the troposphere, with a maximum below 500 hPa. An interesting observation is that, after August 8 when an eyewall replacement cycle takes place, both the APE and KE experience a structure change, each with two maxima in their respective vertical profiles.

The other energetic terms are shown in Fig. 5. Generally speaking, the upper layer and lower layer have completely different scenarios, indicating different mechanisms in different layers co-work to maintain Lekima as a whole. In the upper layer, the budget is mainly between the baroclinic transfer ($\Gamma_A^{0\to1}$), buoyancy conversion (b^1), APE transport ($\nabla\cdot Q_A^1$), and pressure work ($\nabla\cdot Q_P^1$), although some other terms such as barotropic transfer ($\Gamma_K^{0\to1}$) is also significant. Among these processes, the most conspicuous are baroclinic transfer, buoyancy conversion, and pressure work, indicating that here a strong instability occurs, with baroclinic instability dominating. A part of the energy gaining through it is converted into kinetic energy, maintaining the needs for the upper cyclone development. Another part is transported via pressure work downward to supply the needed energy for the cyclone in the lower layer. And, indeed, in the lower layer, the most pronounced process is the (positive) pressure work.

To have a more quantitative view of the above structure, we integrate the energetics as shown in Fig. 5 with respect to p from 975 hPa to 925 hPa and from 225 hPa to 175 hPa, respectively, which are characteristic of the lower-layer and upper-layer dynamics. Note that, when taking integrations, the gravitational acceleration g should be divided to ensure the right unit W/m^2 (Liang, 2016). The resulting integrated energetics are plotted in Fig. 6. Here it is clearer to see that the mechanisms that maintain the cyclonic motions in different layers are quite different. As above, in the lower layer, pressure work contributes positively to maintain Lekima, while in the upper layer, the energy source is mainly from the background APE via baroclinic instability (positive BC, i.e., $\Gamma_A^{0\to1}$) which is subsequently converted into the TC-scale KE via buoyancy conversion (negative b^1).

Recall that around August 8–9 there occurs an eyewall replacement cycle. In the course the TC weakens accordingly. An interesting observation is that, the weakening actually entails a drastic change in the governing dynamics. As clearly displayed in Fig. 5, after that, positive baroclinic transfer ($\Gamma_A^{0\to1}$) begins to be spread all the way down to 1000 hPa (almost through the whole troposphere), and so does the barotropic transfer ($\Gamma_K^{0\to1}$). So the whole air column becomes unstable, with an instability of the mixed type (i.e., both barotropic and baroclinic), in contrast to the previous upper-limited baroclinic instability. Moreover, now the cumulus convection also makes a conspicuous contribution (positive $\Gamma_K^{2\to1}$, upscale transfer), which is also almost through the troposphere. In the mean time, the pressure work becomes greatly increased. Its positivity in the lower layer indicates that the system takes much more energy than before from those acquired via the mixed instability of the background flow. This trend is enhanced after it makes the landfall soon after the eyewall replacement cycle at Wenling, Zhejiang, making an efficient way to supply the energy for it to counteract the dissipation after landing. Notice that these figures reveal that the dynamical processes at the formation stage are essentially weak versions of their corresponding ones before the eyewall replacement cycle.

7 Conclusions

To study the complex multiscale dynamics within the

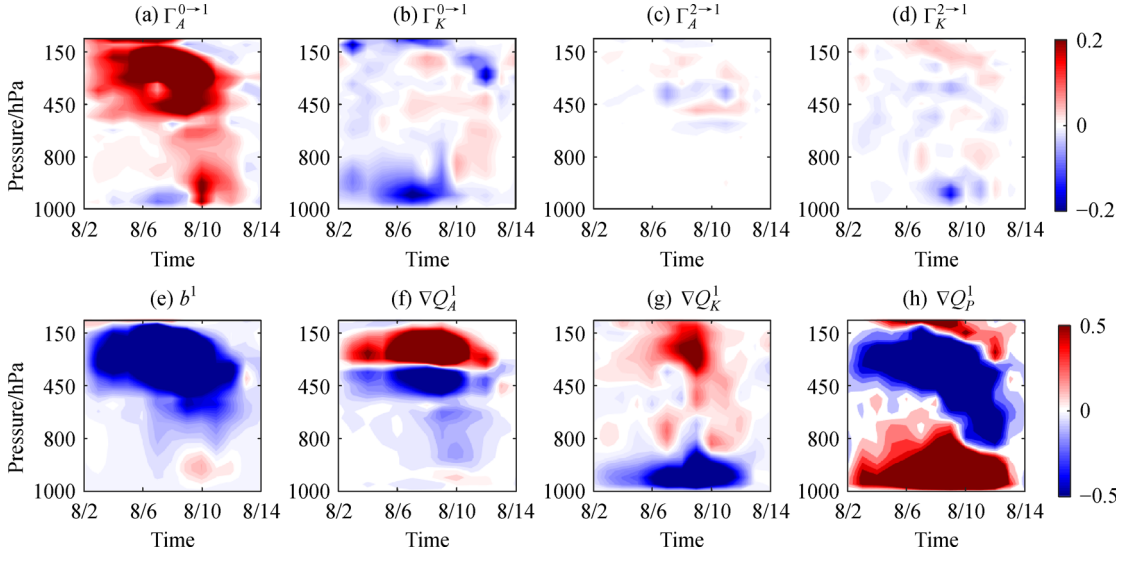

Fig. 5 As Fig. 4, but for $\Gamma_A^{2\to1}$, $\Gamma_K^{0\to1}$, $\Gamma_A^{2\to1}$, $\Gamma_K^{2\to1}$, b^1, $\nabla\cdot Q_A^1$, $\nabla\cdot Q_K^1$ and $\nabla\cdot Q_P^1$.

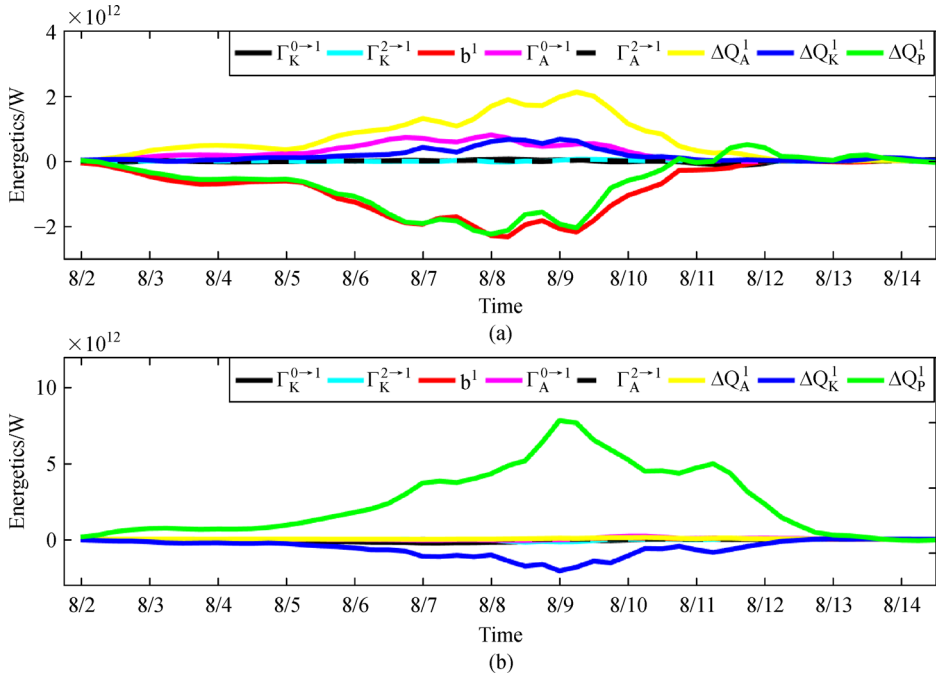

Fig. 6 Time evolutions of the volume integrated TC-scale energetics. (a) Energetics integrated from 225 hPa to 175 hPa; (b) energetics integrated from 975 hPa to 925 hPa (in W).

atmospheric system, recently a mathematical apparatus, called multiscale window transform, or MWT for short, has been developed. Based on it also developed is a methodology for diagnosing localized multiscale energetics and local Lorenz cycles. A key concept is canonical transfer, a faithful representation of the intrinsic processes, which are unobservable but central to the formation of various patterns in fluid flows. This theory and subsequently the methodology have been successfully applied to the investigation of many different geophysical fluid dynamics problems such as atmospheric blocking, MJO, storm track, etc., and the harnessing of vortex shedding in engineering flows (Liang, 2016). In this study, with it we have examined the multiscale dynamical processes underlying Lekima, the second costliest typhoon in the history of China.

We first reconstructed the reanalysis fields from ECMWF onto three scale windows, i.e., the background flow window, the TC-scale window, and the convection-scale window. The reconstruction on the TC window reveals the whole life cycle of Lekima, including the birth, movement, intensification, and decay. The localized energetics analysis allows us to examine the dynamical processes underlying the mobile cyclone, which shows distinctly different scenarios before and after August 8–9, 2019, when an eyewall replacement cycle takes place, and the typhoon makes its first landfall at Wenling, Zhejiang. Before that, in the upper layer the energy growth is largely balanced by baroclinic transfer (positive), buoyancy conversion (negative) and pressure work (negative); in the lower layer it is by the positive pressure work. In other words, the energy supply in the upper layer is mainly through a strong top-limited baroclinic instability; the APE thus-gained is then converted into the TC-scale KE, with a portion to fuel the upper part of Lekima, another portion transported downward to the lower troposphere. The KE transported from above maintains the development of the cyclone in the lower layer.

After Lekima experiences the eyewall replacement cycle and, subsequently, makes the first landfall, a drastic change in dynamics occurs. Though the pressure work is still positive in the lower layer, and negative in the upper layer, it is greatly increased in magnitude. Now positive baroclinic transfer almost spreads throughout the troposphere, and so does barotropic transfer. That is to say, the whole air column is now unstable, with an instability of the mixed type (i.e., both barotropic and baroclinic), in contrast to the previous upper layer-limited baroclinic instability. Moreover, now there occurs an upscale transfer from the cumulus convection. These newly occurred instabilities help to compensate the increasing expense of TC-scale KE by the landfallen Lekima, in order to counteract the topographic irregularity-induced dissipation, and thus maintain a relatively long-lived cyclone over mainland China.

Acknowledgements Thanks are due to ECMWF for making the data available. We appreciate the suggestions from three anonymous reviewers, which helped improve significantly the presentation of the material. This study is partially supported by the National Natural Science Foundation of China (Grant No. 41975064) and the 2015 Jiangsu Program for Innovation Research and Entrepreneurship Groups.

References

Bister M, Emanuel K A (1997). The genesis of hurricane Guillermo: texmex analyses and a modeling study. Mon Weather Rev, 125(10): 2662–2682

Charney J G, Eliassen A (1964). On the growth of the hurricane depression. J Atmos Sci, 21(1): 68–75

Cheung K K W (2004). Large-scale environmental parameters associated with tropical cyclone formations in the western North Pacific. J Clim, 17(3): 466–484

Emanuel K A (1986). An air-sea interaction theory for tropical cyclones. Part I: steady-state maintenance. J Atmos Sci, 43(6): 585–605

Emanuel K A (1989). The finite-amplitude nature of tropical cyclonogenensis. J Atmos Sci, 46(22): 3431–3456

Fei J F, Wu R S, Huang X G, Wang Y, Cheng X (2011). Development of an integrated vertical-slantwise convective parameterization scheme and its associated numerical experiments. Acta Meteorol Sin, 25(4): 405–418

Gray W M (1968). Global view of the origins of tropical disturbances and storms. Mon Weather Rev, 96(10): 669–700

Hendricks E A, Montgomery M T, Davis C A (2004). The role of "vortical" hot towers in the formation of Tropical Cyclone Diana (1984). J Atmos Sci, 61(11): 1209–1232

Li G, Ma J, Liang X (2020). A study of the multiscale dynamical processes underlying the blocking high that caused the January 2008 freezing rain and snow storm in southern China. Acta Meteorol Sin, 78(1): 18–32

Liang X S, Anderson D G M (2007). Multiscale window transform. SIAM Journal on Multiscale Modeling and Simulation, 6(2): 437–467

Liang X S, Robinson A (2007). Localized multiscale energy and vorticity analysis: II. finite-amplitude instability theory and validation. Dyn Atmos Oceans, 44: 51–76

Liang X S (2016). Canonical transfer and multiscale energetics for primitive and quasi-geostrophic atmospheres. J Atmos Sci, 73(11): 4439–4468

Liang X S, Robinson A R (2005). Localized multiscale energy and vorticity analysis: I. fundamentals. Dyn Atmos Oceans, 38(3–4): 195–230

Liu L, Fei J F, Lin X P, Song X, Huang X, Cheng X (2011). Study of the air-sea interaction during Typhoon Kaemi (2006). Acta Meteorol Sin, 25(5): 625–638

Luo Z(2005). Typhoon self-organization in a multi-scale coexpisting system. Acta Meteorologica Sinica, 2005(5): 672–682 (in Chinese)

Luo Z X, Wang Y, Ma G L, Yu H, Wang X W, Sao L F, Li D H (2014). Possible causes of the variation in fractal dimension of the perimeter during the Tropical Cyclone Dan motion. Sci China Earth Sci, 57(6): 1383–1392

Ma J, Liang X S (2017). Multiscale dynamical processes underlying the wintertime atlantic blockings. J Atmos Sci, 74(11): 3815–3831

Maloney E D, Hartmann D L (2001). The Madden-Julian oscillation, barotropic dynamics, and North Pacific tropical cyclone formation. Part I: observations. J Atmos Sci, 58(17): 2545–2558

Ma L M, Tan Z M (2009). Improving the behavior of the cumulus parameterization for tropical cyclone prediction: convection trigger. Atmos Res, 92(2): 190–211

Ma Z. H, Fei J F, Liu L, Huang X G, Cheng X P (2013). Effects of the cold core eddy on tropical cyclone intensity and structure under idealized air-sea interaction conditions. Monthly Weather Review, 141(4):1285–1303

McBride J L, Keenan T D (1982). Climatology of tropical cyclone genesis in the Australian region. Inter J Clim, 2(1): 13–33

Molinari J, Vollaro D, Skubis S, Dickinson M (2010). Origins and mechanisms of eastern Pacific tropical cyclogenesis: a case study. Mon Weather Rev, 128: 2000

Montgomery M T, Nicholls M E, Cram T A, Saunders A B (2006). A vertical hot tower route to tropical cyclogenesis. J Atmos Sci, 63(1): 355–386

Montgomery M T, Sang N V, Smith R K, Persing J (2009). Do tropical cyclone intensity by WHISH? Q J R Meteorol Soc, 135(644): 1697–1714

Montgomery M T, Farrell B F (1993). Tropical cyclone formation. J Atmos Sci, 50(2): 285–310

Ooyama K V (1982). Conceptual evolution of the theory and modeling of the tropical cyclone. J Meteorol Soc Jpn (Ser. II), 60(1): 369–380

Papin P (2011). Using the Rossby radius of deformation as a forecasting tool for tropical cyclogenesis. In: Proceedings of the National Conference on Undergraduate Research, Ithaca, NY, USA

Riehl H (1954). Tropical Meteorology. New York: McGraw Hill Book

Simpson J, Ritchie E, Holland G J, Halverson J, Stewart S (1997). Mesoscale interactions in tropical cyclone genesis. Mon Weather Rev, 125(10): 2643–2661

Wu L, Duan J (2015). Extended simulation of tropical cyclone formation in the western North Pacific monsoon trough. J Atmos Sci, 72(12): 4469–4485

Xu F, Liang X S (2017). On the generation and maintenance of the 2012/13 sudden stratospheric warming. J Atmos Sci, 74(10): 3209–3228

Yu H (1999). A numerical study on the relationship between the asymmetric structure and moving velocity of typhoon in baroclinic atmosphere. Acta Meteorol Sin. 57(6), 694–704

Yang Y, Liang X S (2016). The instabilities and multiscale energetics underlying the Mean–Interannual–Eddy interactions in the Kuroshio extension region. J Phys Oceanogr, 46(5): 1477–1494

Yang Y, Weisberg R H, Liu Y, San Liang X (2020). Instabilities and multiscale interactions underlying the loop current eddy shedding in the Gulf of Mexico. J Phys Oceanogr, 50(5): 1289–1317

Ying M, Zhang W, Yu H, Lu X, Feng J, Fan Y, Zhu Y, Chen D (2014). An overview of the China Meteorological Administration tropical cyclone database. J Atmos Ocean Technol, 31(2): 287–301

Yu H, Wu G (2001). Moist barolinity and abrupt intensity change of tropical cyclone. Acta Meteorol Sin, 59(4): 440–449 (in Chinese)

Zhao Y B, Liang X S (2018). On the inverse relationship between the boreal wintertime Pacific jet strength and storm-track intensity. J Clim, 31(23): 9545–9564

Zhao Y B, Liang XS (2019). Causes and underlying dynamic processes of the mid-winter suppression in the North Pacific storm track. Sci Chn Earth Sci, 62(5): 872–890

Zhao Y B, Liang X S, Guan Z, Hodges K I (2018). The asymmetric eddy-background flow interaction in the north Pacific storm track. Q

J R Meteorol Soc, 145(719): 575– 596

Zhang D L, Bao N (1996). Oceanic cyclogenesis as indued by a mesoscale convective system moving offshore. Part II: genesis and thermodynamic transformation. Mon Weather Rev, 124(10): 2206–2226

Zhang J A, Katsaros K B, Black P G, Lehner S, French J R, Drennan W M (2008). Effects of roll vortices on turbulent fluxes in the hurricane boundary layer. Boundary-Layer Meteorol, 128(2): 173–189

Zhang J A, Robert FRogers, Tallapragada V (2017). Impact of parameterized boundary layer structure on tropical cyclone rapid intensification forecasts in HWRF. Mon Weather Rev, 145(4): 1413–1426

Zong H J, Wu L G (2015). Re-examination of tropical cyclone formation in monsoon thoughs over the western North Pacific. Adv Atmos Sci, 32(7): 924–934